JOURNAL OF MATERIALS SCIENCE 33 (1998) 869–876

Toughening effects of WC/Co particles and compressive surface stress on (Al_2O_3–WC/Co)/TiC/Ni graded materials

J. S. LIN, Y. MIYAMOTO, K. TANIHATA*
*Joining and Welding Research Institute, and *The Institute of Scientific and Industrial Research, Osaka University, Ibaraki, Osaka 567, Japan*
E-mail: miyamoto@jwri.osaki-u.ac.jp

M. YAMAMOTO, R. TANAKA
Japan Ultra High Temperature Material Research Institute, Okiube 573-3, Ube 755, Japan

A graded material of the (Al_2O_3–WC/Co)/TiC/Ni was prepared by using the self-propagating high-temperature synthesis-aided hot isostatic pressing process. The WC/Co particles were added to the outer Al_2O_3 layer in order to activate the heterophase toughening effects and control the thermal expansion mismatch between the outer and inner layers. SEM and TEM observations show a clustering structure of the WC/Co cermet in the Al_2O_3 matrix. The residual stress introduced by the compositionally graded structures was analysed using FEM calculation and X-ray diffraction. Measurements of the indentation toughness and *R*-curve behaviour indicated that the compressive surface stresses and WC/Co particles can significantly strengthen and toughen the Al_2O_3 ceramics. The indentation toughness of the (Al_2O_3–WC/Co)/TiC/Ni at the surface was 13.1 MPa $m^{1/2}$, while those of the (Al_2O_3–WC/Co) uniform composite and the monolithic Al_2O_3 were 7.3 and 4.0 MPa $m^{1/2}$, respectively. It was found by SEM observation of the crack propagation induced by indentation, that the crack deflection, bridging, blunting and arresting occurred at the WC/Co clusters.

1. Introduction

The advantages of layered or graded microstructures to the strength and toughness of ceramics have been manifested in various ceramic systems [1–6]. In the case of surface compressive stress, especially, these advantages are more outstanding. For instance, Lange [4] introduced a compressive surface stress in the Si_3N_4/ZrO_2 ceramics utilizing the volume expansion accompanying the phase change from zirconium oxynitride to monoclinic ZrO_2 in oxidation. In this case, the apparent surface fracture toughness was directly related to the oxidation kinetics and the initial volume content of ZrO_2 that correspond to the surface residual stress. Green [7] developed a Y_2O_3 removal technique for the Y_2O_3-alloyed ZrO_2 ceramics with special heat treatment to promote the transformation of tetragonal ZrO_2 to monoclinic in the surface region and to introduce a compressive surface stress. The indentation experiments confirmed an improvement of the contact resistance of this material.

The deep compressive surface layer is preferable for restraining the initiation or growth of microcracks. As indicated by Virkar *et al.* [5], however, it is difficult to build a deep compression layer by using Lange's or Green's processes. In order to overcome this shortcoming, some layered structures were designed and fabricated in the Al_2O_3/ZrO_2 [5, 8–10], SiC/AlN [11], Al_2O_3/TiC/Ni [6, 12, 13] and $MoSi_2/Al_2O_3$/Ni [14] systems. The compressive stresses were introduced by use of the transformation of unstabilized ZrO_2 to monoclinic phase in the outer layers upon cooling [5, 8–10] or by the mismatch of the thermal expansion between the inner and outer layers [6, 11–14]. All of the results demonstrated the beneficial effects of deep compressive surface stresses on strength and indentation toughness. Recently, Moriguchi *et al.* [15] expanded this concept to fabricate (Al_2O_3–TiC) /TiC/Ni cutting tools with radially graded structure. The cutting life was extended four-fold for cast iron machining compared with the conventional Al_2O_3–TiC ceramic tools.

In this study, an (Al_2O_3–WC/Co) /TiC/Ni symmetrically graded composite was prepared by self-propagating high-temperature synthesis-aided hot isostatic pressing (SHS/HIP) process. The WC/Co particles can enhance the thermal expansion mismatch between the outer and inner layers because their average thermal expansion coefficient is lower than Al_2O_3, and on the other hand, the complex microstructures were also expected to be effective for further toughening of the surface Al_2O_3 layer. The microstructures of the sintered specimens were analysed by SEM and TEM observations. The residual stress and mechanical properties were evaluated experimentally and analytically.

2. Experimental procedure

2.1. Material fabrication

The starting materials used in this research were Al_2O_3, WC/Co, TiC, and Ni powders. As-received Al_2O_3 powder had an average particle size of 0.4 μm, TiC was 1.4 μm, WC/Co and Ni were 1 μm. The powders in the pre-determined composition were wet-mixed by ball milling for over 48 h, and then dried in a vacuum furnace. For all samples, the composition was fixed in intermediate (I) and central (C) layers as shown in Fig. 1. The outer layers (O) were designed to have different WC/Co volume fractions in order to give different thermal expansion coefficient and Young's modulus. The (O) and (I) layers had a thickness of 1 mm, and the (C) layer was 2 mm. The green compact was vacuum sealed into a borosilicate glass capsule with a BN powder bed, then placed into a graphite chemical oven as shown in Fig. 2. The capsulated green compact was embedded in a silicon powder which was used as a fuel for instantaneous heating. For the samples in this study, 40 g silicon powder was added.

In HIP, the chemical oven was heated to 1150 °C when the nitrogen pressure was applied up to 100 MPa. During heating, the silicon powder was ignited by the exothermic reaction of the thermite pellets at about 1030 °C. The temperature in the chemical oven could reach as high as 2500 °C because of the reaction heat of silicon nitriding. The samples were continuously kept at a temperature of 1150 °C for 30 min and then cooled in the furnace.

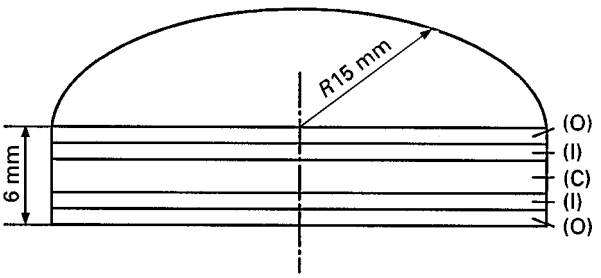

Central layer (C)	TiC+19.8Ni+6.5Mo_2C
Intermediate layer (I)	Al_2O_3+46.8 TiC+2.5Ni
Outer layer (O)	Al_2O_3
	Al_2O_3+(10, 20, 30)WC/Co(23.7)
	Al_2O_3+(10, 20, 30)WC/Co(36.9)

Note: All data in vol %
WC/Co (volume fraction of Co in WC/Co)

Figure 1 Structure and composition of the specimens.

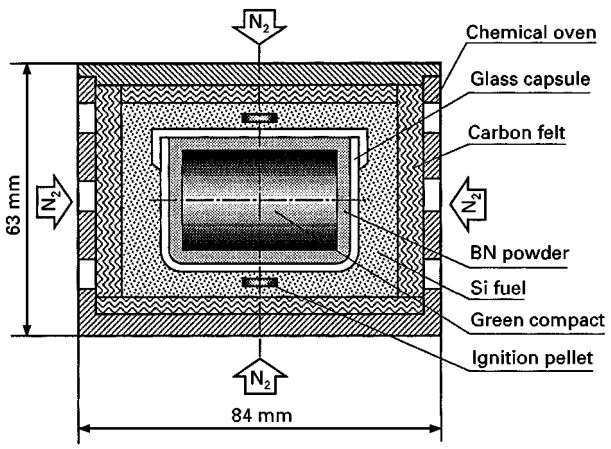

Figure 2 Schematic diagram of the chemical oven used in SHS/HIP sintering.

The layered composites in this paper are denoted FGM, followed by the volume fractions of the WC/Co in the Al_2O_3 surface layer and cobalt in WC/Co, e.g. FGM10(23.7) indicates a surface layer consisting of 10 vol% WC/Co and Al_2O_3, and the volume fraction of cobalt in WC/Co is 23.7%.

2.2. Characterization of graded structures

Microstructural observation was performed on the polished cross-section using scanning electron microscopy (SEM). The outer layer of the specimen FGM20(23.7) was analysed by the transmission electron microscopy (TEM). TEM specimens were prepared via cutting, polishing, dimpling and ion-beam thinning. Hardness and indentation fracture toughness were determined by using a Vickers hardness testing machine with an indentation load of 196 N. The specimens were polished to a diamond surface finish of 3 μm before the test. The indention-induced crack length, $2c$, was measured using an optical microscope and the indentation fracture toughness, K_c, was calculated using the following expression [16]

$$(K_c\phi H_v a^{1/2})\,(H_v/E\phi)^{2/5} = 0.129(c/a)^{-3/2} \qquad (1)$$

where ϕ is a material-independent constant. H_v, E and a are Vickers hardness, Young's modulus and half-diagonal length of the indentation, respectively. The indentation–strength method [17, 18] was used to evaluate the R-curve behaviour of the graded materials. The indentations with loads from 4.9–196 N were made in the centre of a beam $2 \times 6 \times 25\,mm^3$ in size, which subsequently fractured by three-point bending. The indentation strength, crack length and load in bending experiments were used to calculate the R-curve: $K_R = k(\Delta c)^m$, where K_R is the fracture resistance, Δc crack extension and k, m are material constants.

A commercial finite element software MARC was used to analyse the macro-thermal residual stress produced by the graded structures and the micro-thermal residual stress produced by the mismatch of the thermal expansion coefficients of Al_2O_3 ($8.0 \times 10^{-6}\,°C^{-1}$), WC ($4.0 \times 10^{-6}\,°C^{-1}$) and cobalt ($12.3 \times 10^{-6}\,°C^{-1}$). Macro residual stress on the surface of the specimen was determined by the X-ray diffraction method and compared with the results obtained from the finite element method (FEM).

3. Results and discussion

3.1. Microstructure observation

The obtained materials were well densified and showed a uniform microstructure in every layer. Fig. 3 shows scanning electron micrographs of each interfacial zone. In the central layer, the TiC particles (black phase) are surrounded with a layer of grey structure of

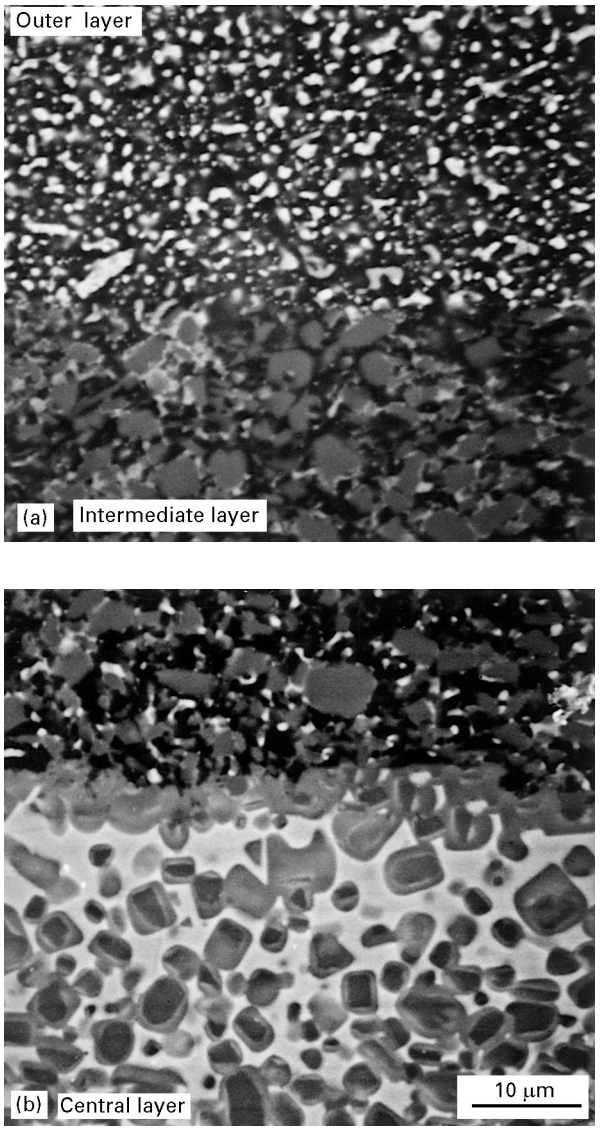

Figure 3 SEM microstructures in (a) the outer layer and intermediate layer and (b) the central layer.

Ti–Mo–C phases. The white phase is nickel. In the intermediate layer, the TiC particles are uniformly distributed in the Al_2O_3 matrix with a little nickel phase. In the outer layer, some WC particles tend to be clustered with the metal cobalt as cementing agent. The clustering of WC and cobalt seems to be due to the poor wetting ability between cobalt and Al_2O_3. From the observation of indention-induced cracks, it was found that the clustered WC/Co islands could effectively restrain the crack propagation.

Fig. 4 shows transmission electron micrographs of the outer layer of FGM20(23.7). It can be seen that the Al_2O_3/WC or Al_2O_3/Co interfaces were well bonded. Isolated WC particles, as seen in Fig. 4a dominantly existed at the grain boundary or grain junctions of the Al_2O_3 matrix, probably to reduce the interface energy. Cobalt was always distributed along the Al_2O_3/WC interface (Fig. 4b) or existed in the cluster of WC particles (Fig. 4c), and no isolated cobalt particles were found in the Al_2O_3 matrix.

3.2. Residual stresses in graded structure

The graded structure can produce a macroscopic residual stress in the specimens because of the thermal

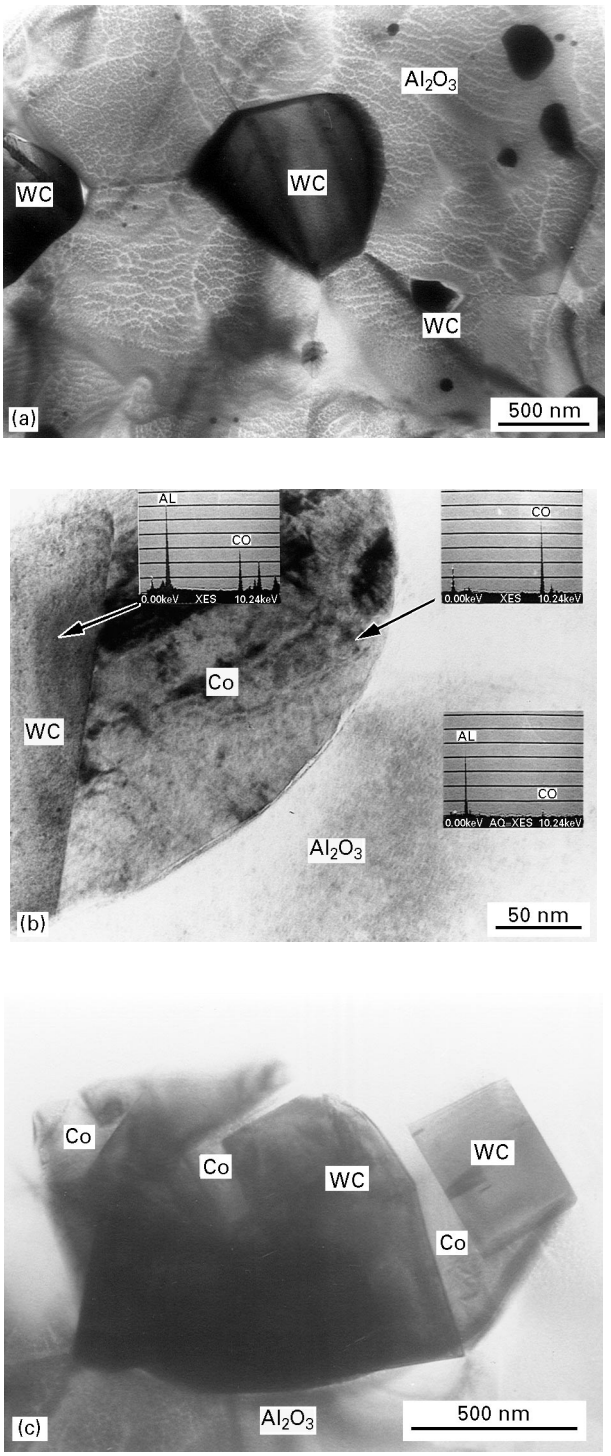

Figure 4 TEM microstructures showing (a) WC particles at the grain boundary and grain junction of the Al_2O_3 matrix, (b) the cobalt phase at the interface between the isolated WC and the Al_2O_3 matrix, and (c) a cluster of WC particles and cobalt metal.

expansion mismatch between neighbouring layers. In this study, FEM analysis was carried out to understand the macro-residual stress induced by graded structures. The modelled configuration of the specimen is shown in Fig. 5. Near the surface and interface the mesh was refined to obtain higher accurate values. A symmetric boundary condition was applied on the boundaries of $X = 0$ and $Y = 0$. Axisymmetric elements were employed in computation supposing a reference temperature of 1150 °C.

Fig. 6a and b illustrate the contour maps of the radial stress and axial stress of FGM20(23.7),

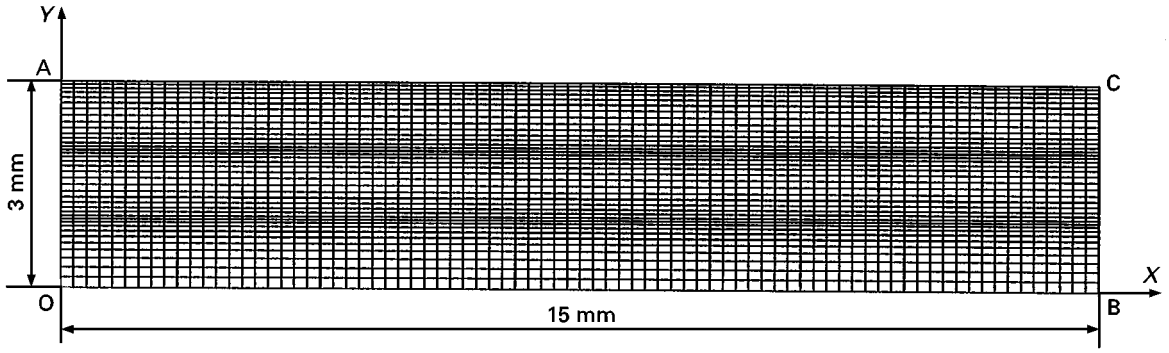

Figure 5 FEM meshes used for the calculation of the residual stress induced by graded structures.

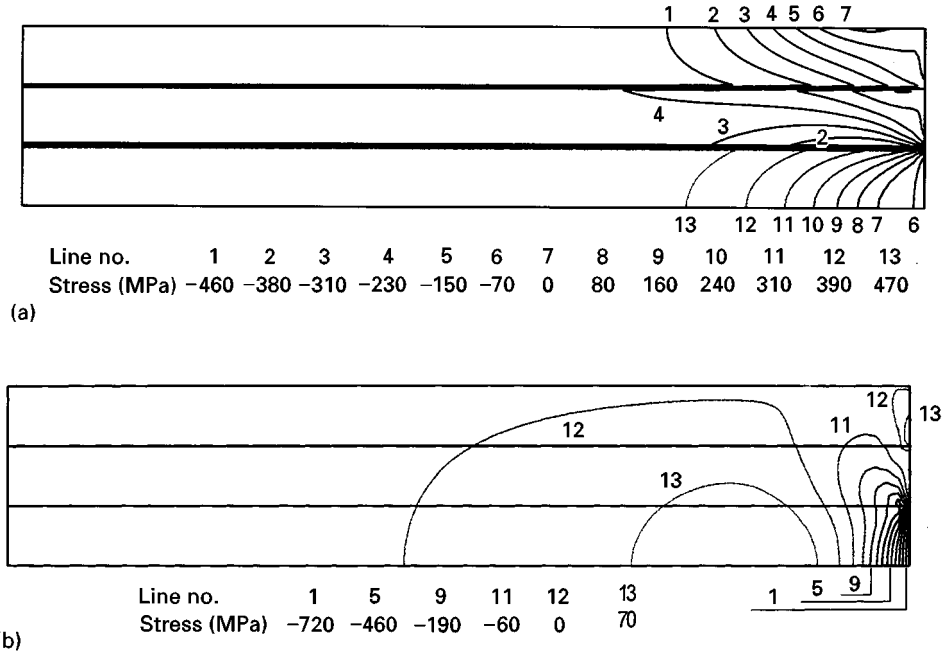

Figure 6 Counter map of thermal residual stress in specimen FGM20(23.7) : (a) radial stress, (b) axial stress.

TABLE I Hardness, flexural strength and surface residual stress of the specimens

Material	Hardness (GPa)	Flextural strength (MPa)	Residual stress (MPa)	
			Measured	Calculated
Monolithic Al_2O_3	18.0	400	0	–
FGM0	20.0	900	−220	−313
FGM10(23.7)	19.8	867	−413	−382
FGM20(23.7)	19.1	952	−465	−453
FGM30(23.7)	18.7	971	−696	−534
FGM10(36.9)	19.1	780	−328	−343
FGM20(36.9)	17.8	670	−403	−376
FGM30(36.9)	18.1	–	−480	−407

respectively. In the outer and intermediate layers, Fig. 6a, a uniform radially compressive stress is developed, except in the edge region, while the central layer sustains a high tensile stress to balance with the compression in the outer and intermediate layers. The residual stress in every layer is nearly constant, except in the edge part. In the central area, a small axial stress (about 3 MPa) is induced owing to the geometric symmetry of the specimen. The maximum of the axial tensile stress occurs in a local area denoted as contour line 13 in Fig. 6b, i.e. about 70 MPa.

The surface residual stresses calculated by FEM and determined by X-ray diffraction are summarized in Table I with the hardness and flexural strength. It can be seen that the compressive surface stress is enhanced significantly as the WC/Co content increases in the outer layer, especially for the materials with a small ratio of cobalt to WC. The X-ray diffraction for WC shows a slightly higher stress than the FEM calculation. It is believed that the microscopic compressive stress subjected by WC particles is responsible for this fact; the compressive stress is

produced by the mismatch of thermal expansion between the WC and Al_2O_3.

3.3. Flexural strength and hardness

As shown in Table I, the compressive surface stress increases strongly as the WC/Co volume fraction increases; however, the response of the flexural strength is not so susceptible. For FGM(23.7), the addition of 30 vol % WC/Co particles into the outer layer makes the compressive surface stress increase by 476 MPa (from 220 MPa to 696 MPa), the flexural strength increase by 71 MPa (from 900 MPa to 971 MPa). In the WC/Co-free case, the flexural strength of the specimen FGM0 with a compressive surface stress of 220 MPa is 900 MPa, increases by 500 MPa (from 400 MPa to 900 MPa).

As described in Section 3.2, in conjunction with the occurrence of the surface compressive stress, a strong tensile stress is developed in the central layer. In the bending experiment, the cumulative result of the applied stress and residual stress will give the maximum tensile stress in the inner layer with the increase in the residual stress, thus resulting in crack initiation from the inner layer, as observed elsewhere [19]. The strengthening effect of the surface compressive stress is reduced.

The hardness at the surface decreases with increasing WC/Co content because of the increase in the cobalt metal. However, hardness values are not lower than that of the monolithic Al_2O_3 ceramic.

3.4. Toughness and *R*-curve behaviour

The indentation fracture toughness is plotted as a function of WC/Co volume fraction in Fig. 7. The surface toughness gradually increases with increasing WC/Co content, but becomes constant for FGM(23.7) or decreases for FGM(36.9) with over 20 vol % WC/Co. The FGM20(23.7) specimen shows a peak toughness of 12.8 MPa $m^{1/2}$, that is 88% higher than the toughness of the FGM0 (6.8 MPa $m^{1/2}$).

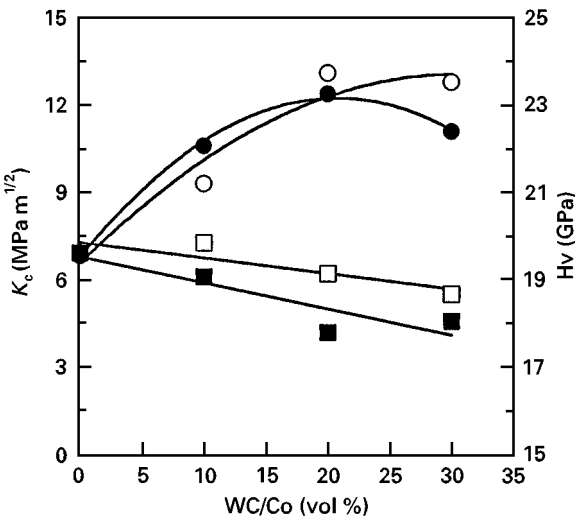

Figure 7 (●, ○) Toughness and (■, □) hardness of graded materials as a function of WC/Co volume fraction: (○, □) 23.7, (○, ■) 36.9.

As compared with Al_2O_3/TiC/Ni (FGM0), the improvement in the indentation toughness of the (Al_2O_3–WC/Co)/TiC/Ni FGM is attributed to the increase in the compressive stress and the dispersion of WC/Co in the surface layer. According to the indentation fracture mechanics for the half-penny-shaped flaw [11, 20], the indentation toughness, K_c, is related to the indentation crack length, c, as follows

$$K_c = \chi \frac{P}{c^{3/2}} + \frac{2}{\pi^{1/2}} \sigma_R c^{1/2} \quad (2)$$

where χ is a constant, P is the indentation load, and σ_R the residual stress. The first term, $\chi(P/c^{3/2})$, is the instrinsic toughness in the state of residual free stress, later denoted as K_0. K_c and $c^{1/2}$ follow a linear relation associated with K_0 and σ_R. Fig. 8 gives plots of

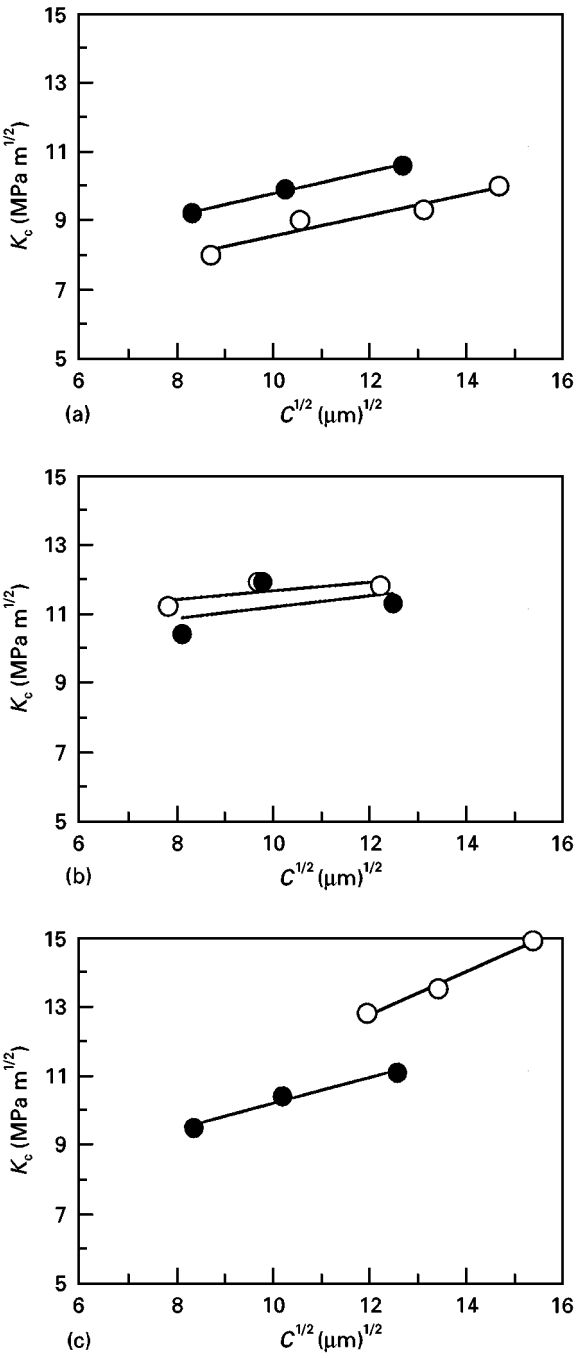

Figure 8 Relation between the indentation toughness and crack length. (a) FGM 10, (b) FGM 20, (c) FGM 30. (○) 23.7, (●) 36.9 cobalt contents.

TABLE II K_0 and σ_R values calculated from Equation 2 with measured K_0

Material	K_0 (MPa m$^{1/2}$)	K_0 (MPa m$^{1/2}$) measured	σ_R (MPa)
FGM0	4.1	4.0	−220
FGM10(23.7)	5.5	5.6	−267
FGM20(23.7)	7.8	7.3	−383
FGM30(23.7)	5.4	6.1	−546
FGM10(36.9)	6.6	–	−283
FGM20(36.9)	7.2	–	−381
FGM30(36.9)	6.5	–	−331

K_c versus $c^{1/2}$ for individual materials. All sets of data can be fitted by straight lines. The values of K_0 and σ_R, which were obtained by linear fitting, are summarized in Table II. Compared with data in Table I, the σ_R values are approximately consistent with the measured values by X-ray diffraction. From K_0 values, the toughening effects of WC/Co particles on the Al_2O_3 matrix is significant, especially for FGM20(23.7), the indentation toughness increases by 90%. Practical indentation tests on uniform (Al_2O_3–20%WC/Co) composite give an indentation toughness of 7.3 MPa, i.e. an increase of 82.5%.

It has been demonstrated that the *R*-curve behaviour exists in various toughened ceramics. The advantage of the surface compression for introducing a steep *R*-curve has been manifested by a three-dimensional finite element analysis [21]. In the present study, an indentation–strength method was used to examine the *R*-curve behaviour of the (Al_2O_3–WC/Co)/TiC/Ni FGMs. The experiments and calculation for *R*-curves were performed following the procedure suggested by Krause [17]. Fig. 9 illustrates the fracture resistance, K_R, versus the crack extension, Δc, based on the exponential function $K_R = k(\Delta c)^m$, where k and m are constants, and m is a measure of susceptibility to the *R*-curve behaviour; both calculated values are listed in Table III. Compared with monolithic Al_2O_3 material, the *R*-curves for the FGMs show

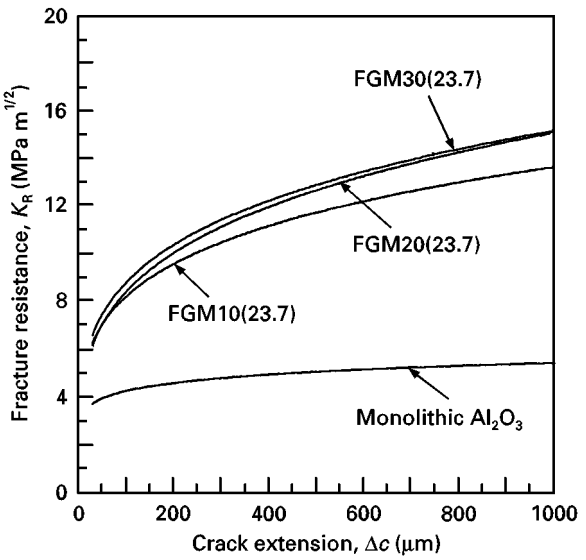

Figure 9 Rising crack-growth resistance curves as a function of crack extension for graded materials and monolithic Al_2O_3.

TABLE III Parameters defining the *R*-curves for graded materials and monolithic Al_2O_3

Material	k	m
Monolithic Al_2O_3	11.9	0.112
FGM10(23.7)	64.2	0.224
FGM20(23.7)	89.4	0.257
FGM30(23.7)	79.8	0.240

a much higher crack extension resistance, i.e. bigger values of k, and excellent damage tolerance, i.e. larger m values.

The addition of WC/Co into the outer Al_2O_3 layer can produce dual effects of enhancing the compressive stress and activating the toughening mechanism due to the dispersion of second-phase particles. The contribution of the compressive surface stress to the indentation toughness, that was described in Equation 2, has been proved by the results as shown in Fig. 8. The effects of WC/Co particles can be revealed by the observation of indentation crack growth. Fig. 10 is a scanning electron micrograph of the crack propagation. It is indicated that the increased toughness associated with WC/Co can be attributed to crack bridging and/or deflection as well as plastic deformation of the cobalt metal which exists at the WC/Al_2O_3 interfaces or in the WC clusters. As a crack reaches the Al_2O_3/WC interface or WC cluster, the high ductility of the cobalt metal leads to crack blunting, as shown in Fig. 11, and/or forces the crack to propagate along the interface.

Utilizing ductile metal inclusions to toughen ceramics has recently attracted attention [22–25]. Because of a considerable mismatch of thermal expansion between the metal inclusions and the ceramic matrices, the ceramic–metal interface is subjected to a radial tensile stress at room temperature. If the size of the metal inclusion is larger than the critical size, cracks will generate at the interface, and the inclusion fails to toughen the ceramics. The texture of cobalt surrounding WC in the Al_2O_3 matrix is expected to be preferable for improving the stress state of the Co/Al_2O_3 interface because of the low thermal expansion of WC. In order to investigate this concept, FEM was used to analyse the residual stress induced by the mismatch of the thermal expansion between WC,

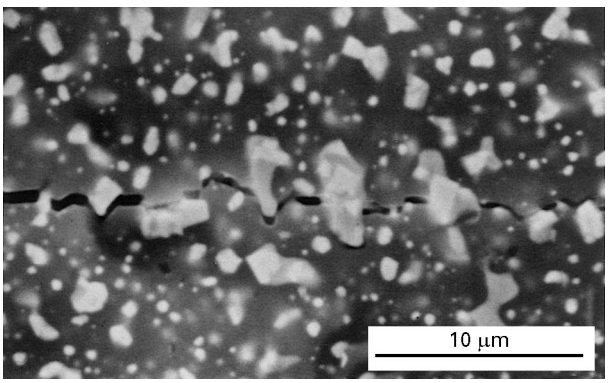

Figure 10 Scanning electron micrograph showing the crack deflection and bridging.

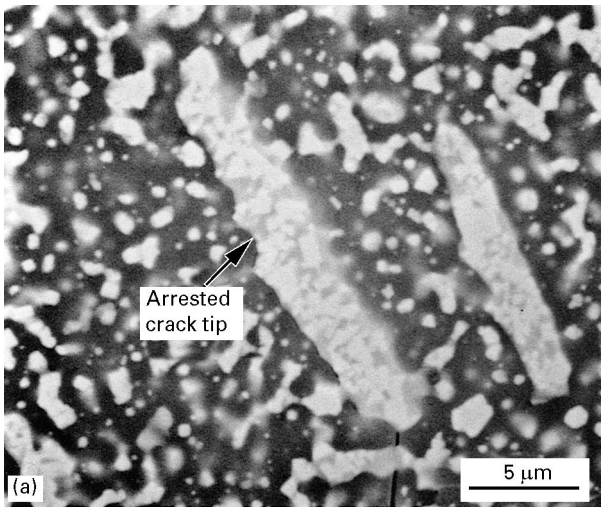

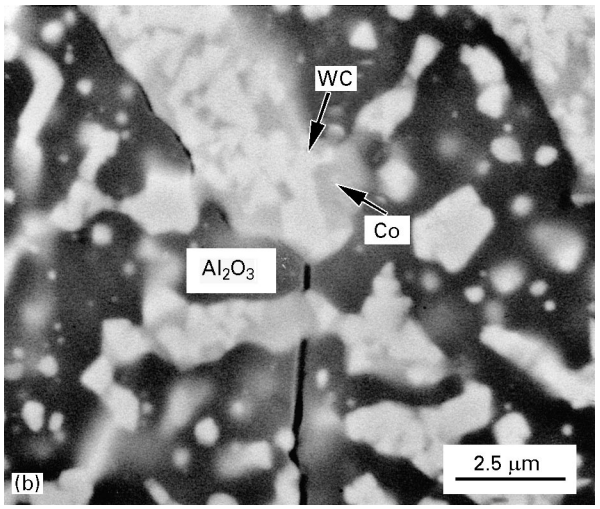

Figure 11 (a,b) Scanning electron micrographs showing crack bridging, blunting and arrest.

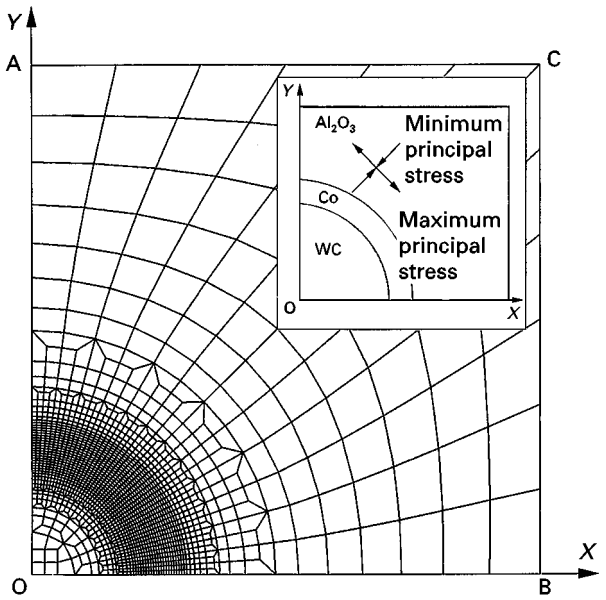

Figure 12 FEM meshes used for the calculation of the residual stress induced by the mismatch of thermal expansion between Al_2O_3, WC and cobalt.

cobalt and Al_2O_3 supposing a temperature drop of 1150 °C. A simple model of a quarter unit cell, as shown in Fig. 12, was used in the computation. A four-node elastic plane stress element for WC and Al_2O_3 and a four-node elastic–plastic plane stress element for cobalt were employed. The reported yield stress of cobalt, 250 MPa, was used as reference.

Fig. 13 shows the distribution of the principal stress as a function of distance from the centre of the WC/Co particle (along line OC in Fig. 12). The direction of the maximum principal stress is parallel to the Co–Al_2O_3 interface, and the minimum stress perpendicular to the interface. A compressive stress exists in the direction perpendicular to the interface, but a strong tensile stress, as high as 400 MPa, occurs in the Al_2O_3 matrix in the direction along the interface. The residual stress in the outer layer should be a summation of the results of the macro- and micro-stresses. When the macro compressive stress exceeds the micro tensile stress, a compressive stress could remain in the matrix, otherwise a tensile stress would appear in the local area. The micro-stress is expected to be dependent on the volume fraction of WC/Co and the volume ratio of cobalt to WC for the present materials. Fig. 14 illustrates the macro compressive stress and micro tensile stress as a function of WC/Co volume fraction. It can be seen that the micro tensile stress tends to

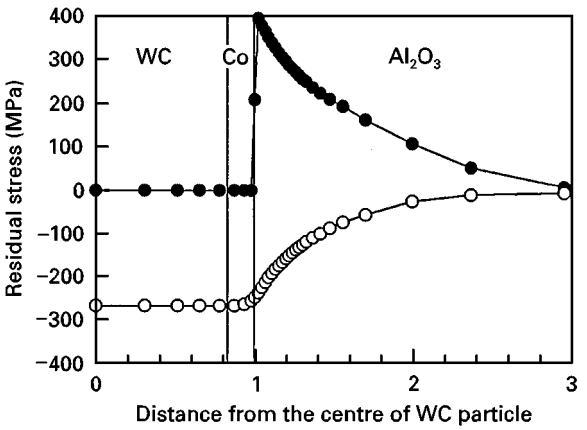

Figure 13 Micro residual stress distribution as a function of the ratio of the distance away from the centre O to the radius WC/Co particle along the line OC in Fig. 12. (●) Maximum principal stress, (○) minimum principal stress.

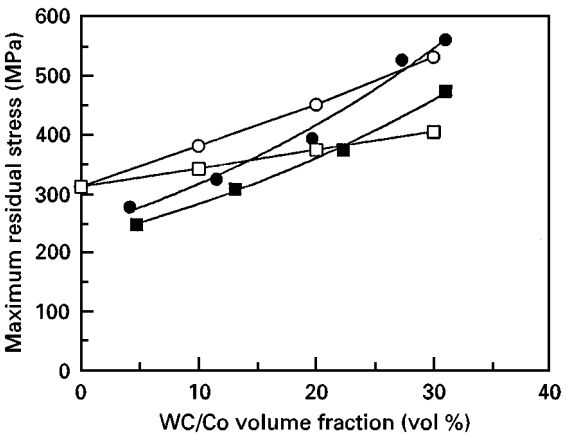

Figure 14 Effect of WC/Co volume fraction on macro and micro residual stress. (○, □) Compressive stress induced by FGM structure. (●, ■) Tensile stress induced by mismatch of thermal expansion of WC/Co/Al_2O_3. (●, ○) FGM (23.7), (■, □) FGM (36.9).

exceed the macro compressive stress when the WC/Co content is over 22 vol % for FGM(36.9) and 27% for FGM(23.7) materials. This result suggests that a local tensile stress would appear in the Al_2O_3 matrix near the Co–Al_2O_3 interface when the volume fraction of WC/Co exceeds 20%, resulting in a reduction of the crack propagation resistance. This may be the reason for the saturation of increasing toughness at 20–30 vol % WC/Co as seen in Fig. 7.

4. Conclusions

1. Symmetrically graded structures can effectively control the stress state on the surface of ceramics via tailoring the mismatch of the thermal expansion. The residual surface compression can develop a steep *R*-curve behaviour in ceramics, and significantly enhance the crack growth resistance and damage tolerance.

2. The WC particles tended to form clusters with cobalt in the Al_2O_3 matrix. Both the strength and toughness of (Al_2O_3–WC/Co)/TiC/Ni materials were remarkably improved because of the dual effects of the surface compressive stress induced by the symmetrically graded structure and the dispersion of secondary phase particles.

3. The FEM analysis showed that the addition of WC/Co to the outer Al_2O_3 layer produced the micro tensile stress at the Co–Al_2O_3 interface in the Al_2O_3 matrix when the WC/Co content increased to 20–30 vol %. A greater volume of WC/Co reinforcements would reduce their effectiveness for toughening Al_2O_3.

Acknowledgement

This study was partly supported by the fund of materials engineering from Nippon Sheet Glass Co. Ltd.

References

1. M. P. HARMER, H. M. CHAN and G. A. MILLER, *J. Amer. Ceram. Soc.* **75** (1992) 1715.
2. D. B. MARSHALL, J. J. RATTO and F. F. LANGE, *ibid.* **74** (1991) 2979.
3. P. SAJGALIK, Z. LENCES and J. DUSZA, *J. Mater. Sci.* **31** (1996) 4837.
4. F. F. LANGE, *J. Amer. Ceram. Soc.* **63** (1980) 38.
5. A. V. VIRKAR, J. L. HUANG and R. A. CUTLER, *ibid.* **70** (1987) 164.
6. Y. MIYAMOTO, Z. LI, Y. S. KANG and K. TANIHATA, *Powder Powder Metall.* **42** (1995) 933 (in Japanese).
7. D. J. GREEN, *J. Amer. Ceram. Soc.* **66** (1983) C178.
8. R. A. CULTER, J. D. BRIGHT, A. V. VIRKAR and D. K. SHETTY, *ibid.* **70** (1987) 714.
9. A. V. VIRKAR, J. F. JUE, J. J. HANSEN and R. A. CULTER, *ibid.* **71** (1988) C148.
10. J. J. HANSEN, R. A. CUTLER, D. K. SHETTY and A. V. VIRKAR, *ibid.* **71** (1988) C501.
11. R. SATHYAMOORTHY, A. V. VIRKAR and R. A. CUTLER, *ibid.* **75** (1992) 1136.
12. Y. MIYAMOTO, Z. LI, Y. KANG and K. TANIHATA, *Int. J. SHS* **5** (1996) 69.
13. Y. MIYAMOTO, K. TANIHATA, Z. LI, Y. S. KANG, K. NISHIDA and T. KAWAI, in "Proceedings of the 8th CIMTEC Conference on Advances in Science and Technology" edited by P. Vincentini, vol. 4 (Techna, Florence, 1995) pp. 387.
14. Y. S. KANG, Y. MIYAMOTO, Y. MURAOKA and O. YAMAGUCHI, *J. Soc. Mater. Sci. Jpn* **44** (1995) 705 (in Japanese).
15. H. MORIGUCHI, A. IKEGAYA, T. NOMURA, Y. MIYAMOTO, Z. LI and K. TANIHATA, *Powder Powder Metall.* **42** (1995) 1389 (in Japanese).
16. K. NIIHARA, R. MORENA and D. P. H. HASSELMAN, *J. Amer. Ceram. Soc.* **65** (1982) C116.
17. R. F. KRAUSE, *ibid.* **71** (1988) 338.
18. Y. W. KIM and M. MITOMO, *J. Mater. Sci.* **30** (1995) 4043.
19. K. TANIHATA, Z. LI and Y. MIYAMOTO, *J. Soc. Mater. Sci. Jpn* **45** (1996) 599 (in Japanese).
20. D. B. MARSHALL and B. R. LAWN, *J. Mater. Sci.* **14** (1979) 2001.
21. R. LAKSHMINARAYANAN, D. K. SHETTY and R. A. CUTLER, *J. Amer. Ceram. Soc.* **79** (1996) 79.
22. V. V. KRSTIC, P. S. NICHOLSON and R. G. HOAGLAND, *ibid.* **64** (1981) 499.
23. W. H. TUAN and R. J. BROOK, *J. Eur. Ceram. Soc.* **6** (1990) 31.
24. W. H. TUAN, H. H. WU and T. J. YANG, *J. Mater. Sci.* **30** (1995) 855.
25. R. KOLHE, C. Y. HUI, E. USTUNDAG and S. L. SASS, *Acta Mater.* **44** (1996) 279.

Received 7 May
and accepted 24 September 1997